Rapid Probing of Glucose Influx into Cancer Cell Metabolism

Using Adjuvant and a pH-Dependent Collection of Central Metabolites to Improve In-Cell D-DNP NMR

Sannelli, Francesca; Wang, Ke-Chuan; Jensen, Pernille Rose; Meier, Sebastian

Published in:
Analytical Methods

Link to article, DOI:
10.1039/D3AY01120H

Publication date:
2023

Document Version
Peer reviewed version

ARTICLE

Rapid Probing of Glucose Influx into Cancer Cell Metabolism: Using Adjuvant and a pH-Dependent Collection of Central Metabolites to Improve In-Cell D-DNP NMR

Received 00th January 20xx,
Accepted 00th January 20xx

DOI: 10.1039/x0xx00000x

Francesca Sannelli,[a] Ke-Chuan Wang,[b] Pernille Rose Jensen,[b] and Sebastian Meier[a*]

Changes to metabolism are a hallmark of many diseases. Disease metabolism under physiological conditions can be probed in real time with in-cell NMR assays. Here, we pursued a systematic approach towards improved in-cell NMR assays. Unambiguous identifications of metabolites and of intracellular pH are afforded by a comprehensive, downloadable collection of spectral data for central carbon metabolites in the physiological pH range (4.0-8.0). Chemical shifts of glycolytic intermediates provide unique pH dependent patterns akin to a barcode. Using hyperpolarized $^{13}C_1$ enriched glucose as the probe molecule of central metabolism in cancer, we find that early glycolytic intermediates are detectable in PC-3 prostate cancer cell lines, concurrently yielding intracellular pH. Using non-enriched and non-enhanced pyruvate as an adjuvant, reactions of the pentose phosphate pathway become additionally detectable, without significant changes to the barriers in upper glycolysis and to intracellular pH. The scope of tracers for in-cell observations can thus be improved by the presence of adjuvants, showing that a recently proposed effect of pyruvate in the tumor environment is paralleled by a rerouting of cancer cell metabolism towards producing building blocks for proliferation. Overall, the combined use of reference data for compound identification, site specific labelling for reducing overlap, and use of adjuvant afford increasingly detailed insight into disease metabolism.

1. Introduction

Intracellular biochemistry plays a decisive role both for biomedicine and for future sustainable production. Therefore, recent years have seen a renewed interest in metabolism and its analysis.[1–4] The direct observation of ongoing cellular biochemistry relies on non-invasive high-resolution observations with spectroscopic methods that do not interfere with cell membranes or cell walls. All these prerequisites are met by NMR spectroscopy. In-cell NMR spectroscopy benefits from compounded improvements in methodology and instrumentation, including hyperpolarized probe molecules,[5–7] improved hardware for enhancing nuclear spin polarization,[8] and cryogenically cooled detection electronics.[9]

The objective for in-cell spectroscopy is usually different from metabolite characterization in metabolomics approaches on stable samples, whose pH value and temperature can be chosen for analysis.[10–12] The intracellular pH is not necessarily known and varies greatly between different intracellular compartments.[13] Protonation and deprotonation largely affect the electron cloud and hence the nuclear shielding in molecules, thus leading to pH effects on chemical shifts.[14] NMR detection of metabolites usually encompasses the detection of ^{1}H[15–18] or ^{13}C[19–21] nuclei, where the former benefits from a high sensitivity

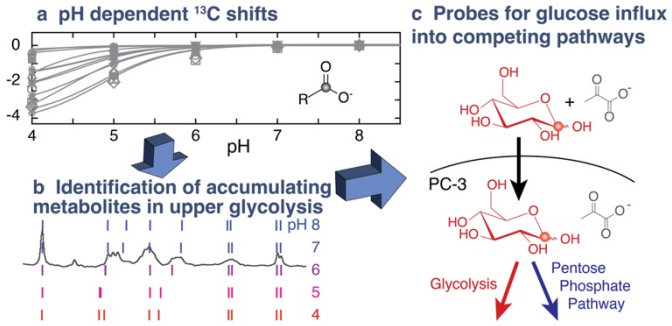

Scheme 1 Obstacles of in-cell NMR assays were addressed herein with pH dependent chemical shift reference data to alleviate identification of intracellular metabolites from single chemical shifts (a). Site specific labelling in conjunction with the chemical shift collection then allowed identifications of intracellular pH and accumulating intermediates of upper glycolysis on the seconds timescale (b). This assay could be improved by the presence of additives in the substrate preparation. Metabolite additives were shown to populate additional pathways in glucose metabolism by cancer cells (c).

[a] Department of Chemistry Technical University of Denmark Kemitorvet, Bygning 207, 2800 Kgs. Lyngby, Denmark; E-mail: semei@kemi.dtu.dk
[b] Department of Health Technology Technical University of Denmark Elektrovej 349 2800-Kgs. Lyngby, Denmark

† Footnotes relating to the title and/or authors should appear here.
Electronic Supplementary Information (ESI) available: See DOI: 10.1039/x0xx00000x
Reference spectra at varying pH values are available as raw data under xx

for mixture analysis, while the latter is currently more suitable for the selective detection of probe molecules through ^{13}C enrichment and hyperpolarization approaches. Hyperpolarization methods in NMR spectroscopy can temporarily redistribute nuclear spin states by more than four orders of magnitude, resulting in enhanced NMR signals during lifetimes that are determined by the T_1 time.[22–25] Intracellular probing using ^{13}C NMR benefits from the large chemical shift range of ^{13}C relative to ^{1}H, from sharp singlet signals in decoupled spectra, and from the low natural abundance of ^{13}C in the cellular background. Especially the isotope- and polarization enriched C1 position in glucose bears great promise for probing central carbon metabolism inside cancer cells: this position is converted to an especially large variety of functional groups in glycolysis and the pentose phosphate pathway. Some cancer cells exhibit notoriously high activities for these pathways.

While hyperpolarized NMR bears promise for characterizing disease metabolism, some obstacles have persisted. These obstacles include (i) problems in the identification of intracellular metabolite signals due to the poorly defined intracellular pH, (ii) overlap of metabolite signals with strong, hyperpolarized substrate signals, and (iii) a limitation to fast metabolic pathways that yield significant substrate conversion on the T_1 time scale, typically of less than one minute.

Here, we systematically address these obstacles: In-cell identification is improved with pH dependent chemical shift data of metabolites (Scheme 1a). These data are shown to afford unambiguous identification of intracellular metabolites in upper glycolysis and of intracellular pH in PC-3 cancer cells if site specific labelling is used to minimize the overlap of metabolite signals with hyperpolarized D-[1-^{13}C,1-^{2}H]glucose substrate (Scheme 1b). Including a non-detected additive in the substrate can finally be shown to accelerate D-[1-^{13}C,1-^{2}H]glucose influx into the pentose phosphate pathway (PPP), rendering both Embden-Meyerhof-Parnas (EMP) glycolysis and the oxidative part of the PPP in cancer metabolism detectable on the assay time scale (Scheme 1c). This observation is significant, as pyruvate secreted in the tumor microenvironment has recently been shown to promote the proliferation of multiple cancer cell types, including pancreatic cancer, in a redox-dependent manner.[26–28] We find that pyruvate affects D-[1-^{13}C,1-^{2}H]glucose influx into different pathways in PC-3 metabolism, indicating an effect of pyruvate accumulation on cancer metabolism due to increased uptake into cellular pools[29] and/or accordingly altered cellular redox state.[30]

2. Experimental Section

2.1 Chemicals and pH variant reference samples

Chemicals were ordered from Sigma Aldrich (Andover, MA, USA) and were used without further purification. Reference samples at pH 4.0 were prepared by dissolving 3-5 mg or 3.5 μL of the compounds in 550 μL of 20 mM Acetate buffer in D_2O (mix of Sodium Acetate and Acetic acid glacial, containing 30 mM ethanol, pH 4.0). Reference samples at pH 5.0, pH 6.0 and pH 7.0 were prepared by dissolving 3-5 mg or 3.5 μL of the compounds in 550 μL of 20 mM MES buffer in D_2O (containing 30 mM ethanol). Reference samples at pH 8.0 were acquired by dissolving 3-5 mg or 3.5 μL of the compounds in 550 μL of 20 mM phosphate buffer in D_2O (Sodium dihydrogen phosphate monohydrate, containing 30 mM ethanol, pH 8.0). The pH values of the solutions of reference compounds were adjusted to 4.0, 5.0, 6.0, 7.0 or 8.0 with a Radiometer Analytical PHC3006-9 Combination pH Electrode with long length (glass body, length 150 mm, diameter 6.5 mm) and a Radiometer Analytical PHM210 standard pH meter. The ethanol chemical shifts were themselves referenced to sodium trimethylsilylpropane-sulfonate (DSS) in a sample containing DSS and ethanol at 30 mM concentration and the desired pH. Multiplicity edited ^{1}H-^{13}C HSQC spectra and ^{1}H-^{13}C HMBC for these authentic standard samples were acquired on an 800 MHz Bruker Avance III HD instrument equipped with a 5 mm TCI cryoprobe and a SampleJet sample changer at 310 K. Multiplicity-edited ^{1}H-^{13}C HSQC spectra were acquired by sampling the FID in the direct and indirect dimensions for 213 and 54 ms, respectively, while ^{1}H-^{13}C HMBC spectra were acquired by sampling the FID in the direct and indirect dimensions for 213 and 6 ms, respectively. These NMR spectra are provided as a downloadable collection (https://doi.org/10.11583/DTU.c.6382923). A colorimetric enzyme kit for the quantification of NAD^+/NADH was obtained from Sigma Aldrich.

2.2 Salt Dependency

Samples containing 0 mM, 100 mM, 200 mM, 400 mM of KCl were prepared in 20 mM MES buffer pH 7.0 in D_2O containing 30 mM ethanol. Amounts of 2-7 mg of metabolite (based on the molecular weight to obtain 40 mM of compound in the sample) were dissolved in the 20 mM MES buffer pH 7.0 in D_2O containing different salt concentrations prior to adjusting the pH values of the solutions to 7.0. The ethanol chemical shifts were referenced in a sample containing DSS and ethanol at 30 mM concentration at pH 7.0. ^{1}H-^{13}C HSQC and ^{1}H-^{13}C HMBC spectra were acquired on an 800 MHz Bruker Avance III HD instrument equipped with a 5 mm TCI cryoprobe and a SampleJet sample changer at 310 K, in 5 mm NMR tubes (KCl concentrations up to 100 mM) or 3 mm NMR tubes (KCl concentrations 200 mM and 400 mM).

2.3 Cell Culture

PC-3 cells (America Tissue Culture Collection) were cultured in RPMI 1640 medium with 10% fetal bovine serum (FBS), 100 units/mL penicillin, 100 mg/mL streptomycin, 2 g/L glucose, and 0.3 g/L L-glutamine (Sigma-Aldrich, St. Louis, MO) at 37 °C in a 5% CO_2 atmosphere. For D-DNP-NMR experiments of metabolism in the presence and in the absence of pyruvate, cells were grown in T175 flasks prepared by seeding 4×10^6 cells. After 6 days 20×10^6 cells were harvested by trypsination, washed in PBS buffer, and resuspended to 200 μL phosphate buffer (40 mM, pH 7.4). Sodium pyruvate was added from a 240 mM stock solution to a final concentration of 20 mM, and the solution was transferred to a Shigemi tube fitted with an injection line.

2.4 Hyperpolarization

Hyperpolarization of D-[1-^{13}C,1-^{2}H]glucose was performed similarly to a previously established protocol for D-[U-^{13}C,U-^{2}H]glucose:[31] briefly, solid state dynamic nuclear polarization was conducted by mixing D-[1-^{13}C,1-^{2}H]glucose with trityl radical OX063 (27 mM; Oxford Instruments, Abingdon, UK) and gadoteridol (1.5 mM; Bracco Imaging, Italy) dissolved in ultra-pure water. The final substrate samples contained 50 μmol D-[1-^{13}C,1-^{2}H]glucose in 19 mg of the sample preparation. The sample was directly placed in a sample cup for hyperpolarization and transferred to a Hypersense polarizer operating at 1.2 K, using microwave irradiation at 94.049 GHz with 100 mW in a magnetic field of 3.35 T for one hour to yield solid-state polarizations above 30%. This determination was based on measured liquid-state polarization (16 %), obtained after a manual transfer time of 10 s. The liquid-state T_1 of was determined to 15 s. The standard deviation for solid state polarization, transport, injection and cell metabolism has previously been determined to 8 % for the same configuration of polarizer and NMR magnet.[32]

2.5 D-DNP NMR

Upon hyperpolarization, 5 ml phosphate buffer (40 mM, pH 7.4) in H_2O was heated to 10 bar and after dissolution the solution was collected in a 50 mL receive container at the neck of the polarizer. Of the dissolved sample 0.33 mL were manually injected into 0.2 mL of a PC-3 cell suspension (kept in H_2O buffer), equilibrated to 310 K inside a 500 MHz Bruker spectrometer that was equipped with a 5 mm DCH CryoProbe and a 11.7 T UltraShield magnet. Metabolism was followed by a series of ^{13}C NMR spectra acquired with an excitation pulse of approximately 12°. Pseudo-2D spectra using a receiver gain of 10 were used to acquire the ^{13}C FID for 344.7 ms every 0.5 s, sampling 11,264 complex data points for acquisition. Data acquisition was started prior to substrate injection to minimize experimental dead-time. The data were processed with zero filling to 32,768 complex data points in Bruker Topspin 4.1.3. An exponential window function with 10 Hz line broadening (LB) was used.

2.6 Statistical Analysis and Plotting

All spectra were analysed in Bruker Topspin 4.1.3. Chemical shift data were plotted using pro Fit 7 (QuantumSoft, Zurich, Switzerland). The pH dependent observed chemical shift values $\delta^{13}C_{obs}$ were fitted to the Henderson-Hasselbalch equation as a guide to the eye (Fig. 5) as

$$\delta^{13}C_{obs} = (\delta^{13}C_{HA} \times 10^{pKa\text{-}pH} + \delta^{13}C_{A^-})/(1 + 10^{pKa\ -\ pH}),$$

where $\delta^{13}C_{HA}$ and $\delta^{13}C_{A^-}$ are the ^{13}C chemical shifts of the metabolite acid and base form at low and high pH, respectively.

3. Results and Discussion

3.1 Systematic trends in metabolite ^{13}C chemical shifts depending on ion concentrations

A principal problem in the identification of intracellular metabolites entails that the intracellular pH is not easily controlled by the experimentalist and is neither homogeneous in the intracellular space nor always constant over time in the cytosol. Accordingly, pH dependent chemical shift changes[33–35] for some of functional groups such as phosphoester groups in upper glycolysis can be too big to warrant identifications at unknown intracellular pH.[36] Accurate pH dependent chemical shift collections were thus deemed necessary for a broad applicability of intracellular ^{13}C NMR, for instance to advance mechanistic understanding in biomedicine and bioproduction. By contrast, current chemical shift collections are mostly compiled for metabolomics studies of biofluids[37] at well-defined pH values (7.0 or 7.4).[10] The most relevant extracellular biomarkers in biofluids are often different from intracellular intermediates of central metabolism. Due to the limited focus on intracellular metabolites, more than ten intermediates of glycolysis and citric acid cycle or adjacent reactions were found to be absent altogether or present with implausible (i.e., unexpected, or contradictory) chemical shift values in current databases.[10] Similarly, literature data often showed discrepancies in the chemical shift data far beyond expected experimental errors, with deviations from plausible values reaching more than 10 ppm in some instances due to errors in site-specific assignments.[38]

Intracellular pH is thought to vary in the pH range of approximately 4.0-8.0 in different cellular compartments. A set of reference compounds encompassing the intermediates of central carbon metabolism was collected with consistent referencing of ^{1}H and ^{13}C chemical shifts to DSS. Spectral data (^{1}H-^{13}C HSQC and ^{1}H-^{13}C HMBC) are provided for download as reference compounds intended for in-cell NMR applications in the pH range of 4.0-8.0. More than 1400 unique chemical shifts were assigned and are collected in Table 1. The collection included metabolites that are of high-concentration inside cells[39] and that hence are most likely candidates for in-cell NMR detection, both with conventional and D-DNP NMR. In addition, metabolites were included for a detoxification route of acetaldehyde that has been described to occur in mammalian liver.[40] This pathway encompasses only compounds without functional groups that are ionizable in the physiological pH range. Hence, these metabolites were used to estimate that chemical shift determinations for reference compounds were conducted with accuracies below 0.002 ppm and 0.02 ppm for ^{1}H and ^{13}C, respectively, when detecting ^{13}C indirectly in suitably sampled heteronuclear 2D NMR spectra.[41,42] In comparison, an accuracy in chemical shift determination of 0.2 ppm for ^{13}C is considered viable in inter-laboratory comparisons.[43,44]

Inspection of the pH dependence of chemical shifts between pH 4.0 and 8.0 showed that the shielding and hence chemical shift in many metabolites is pH independent. Such pH independence applies to metabolites that do not contain ionizable carboxylic acid and phosphoester groups (such as carbohydrates, aldehydes, and alcohols). In addition, α-ketoacids did not show any significant pH dependence in chemical shifts between pH 4.0-8.0 (Fig. S1). The pK_a values for α-ketoacids (such as pyruvic acid, α-ketoglutaric acid and oxaloacetic acid) fall in the range 2.2-2.5, thus leading to no significant protonation at pH values above 4.0. In consequence,

polyols, aldehydes, alcohols and α-ketoacids are viable internal reference compounds with pH invariant ^{13}C chemical shifts. Among these compounds, especially pyruvate has been reported as one of the more highly concentrated metabolites in immortalized mammalian cells,[39] thus suggesting that pyruvate could be a particularly suitable internal reference compound for chemical shift calibration in living cells.

By contrast, the pH dependence of other carboxylic acid and phosphoester containing metabolites showed systematic pH dependent chemical shift changes as evident in Fig. 1. Such chemical shift changes reached ±5 ppm over the physiological pH range (~4.0-8.0). Some of the largest pH variability of metabolite ^{13}C NMR signals was observed for the α,β unsaturated acids phosphoenolpyruvate and itaconic acid. Particularly the carbon in β-position to the carboxylic acid group becomes increasingly deshielded in these compounds upon acidification. All other ^{13}C sites in phosphoenolpyruvate and itaconic acid become increasingly shielded upon acidification (Fig. 1A).

Phosphorylated metabolites showed significant pH-dependent ^{13}C chemical shift changes near physiological pH owing to the pK_a values near 6.0 for the phosphate groups,[14] thus making phosphorylated metabolites a sensitive pH indicator in ^{13}C NMR at weakly acidic pH as expected.[14,45] In contrast to 2-phosphoenolpyruvate, all aliphatic carbons in α position to phosphorylated sites became increasingly shielded (by 0 to -2 ppm between pH 8.0 and pH 4.0) upon acidification (Fig. 1B). The phosphorylated carbon itself became increasingly deshielded (by 0-1.6 ppm between pH 8.0 and pH 4.0), except for 2-phosphoenolpyruvate (Fig. 1C). Finally, all carboxylic acid acids showed shielding of the carboxyl carbons upon acidification (by 0 to -4 ppm between pH 8.0 and pH 4.0, Fig. 1D). Thus, pH effects on metabolite ^{13}C chemical shifts tend to follow patterns that make pH responses qualitatively predictable for different structural motifs. Variability of metabolite ^{13}C NMR chemical shifts in the physiological range indicated, however, that the unambiguous identification of intracellular metabolites from ^{13}C NMR often requires reliable estimates of the intracellular pH, or the determination of multiple chemical shifts for the suspected metabolites.

The changes in ^{13}C and ^{1}H chemical shifts upon acidification from samples with pH 8.0 is summarized in Fig. 2. Fig. 2A shows changes in ^{13}C chemical shift compared to the variance of 0.2 ppm that has been considered realistic with similar referencing.[44] Chemical shift changes from 10^{-8} M to 10^{-7} M H_3O^+ (acidification from pH 8.0 to pH 7.0) often transgress 0.2 ppm, thus corroborating the need for pH dependent chemical shift values for analyte identifications inside cells even near neutral pH. The distribution of chemical shift changes grows when increasing the hydronium concentration from 10^{-7} M to 10^{-6} M and for subsequent tenfold increases in hydronium concentration (Fig. 2). Upon slight acidification from 10^{-7} M to 10^{-6} M H_3O^+ (pH 7.0 to pH 6.0), approximately 30% of all ^{13}C chemical shifts were found to change by more than 0.2 ppm. The variation in ^{13}C chemical shifts upon acidification was approximately 20-fold larger than the variation in ^{1}H chemical shifts (Fig. 2 and Fig. S2), consistent with the approximately 20-fold larger overall chemical shift range in ^{13}C NMR relative to ^{1}H NMR.

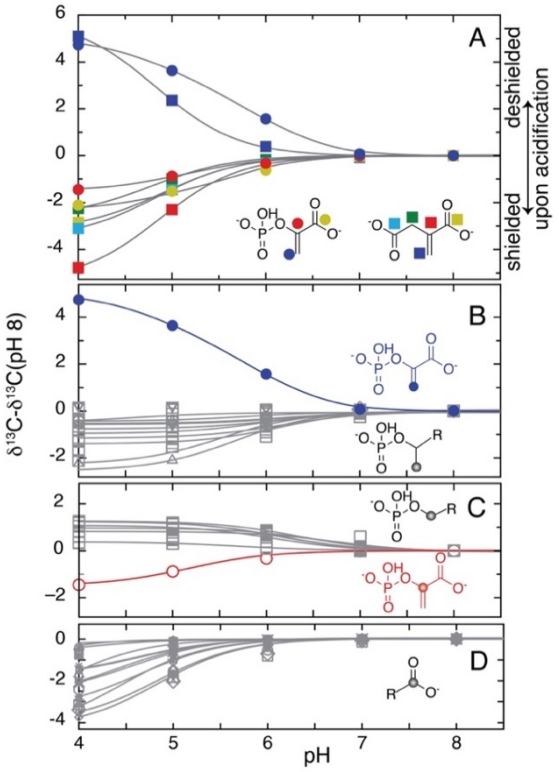

Fig. 1 The pH dependence of ^{13}C chemical shifts in metabolites containing carboxylic acid or phosphoester groups in the indicated structural motifs (A: α,β unsaturated carboxylic acid, B: ^{13}C adjacent to phosphoester – comparison between phosphoenolpyruvate and aliphatic phosphoesters, C: ^{13}C in phosphoester – comparison between phosphoenolpyruvate and aliphatic phosphoesters, D: carboxylic acid group, not adjacent to carbonyl or olefinic group). Changes relative to the ^{13}C chemical shifts at pH 8.0 are plotted, with positive values corresponding to deshielding upon acidification.

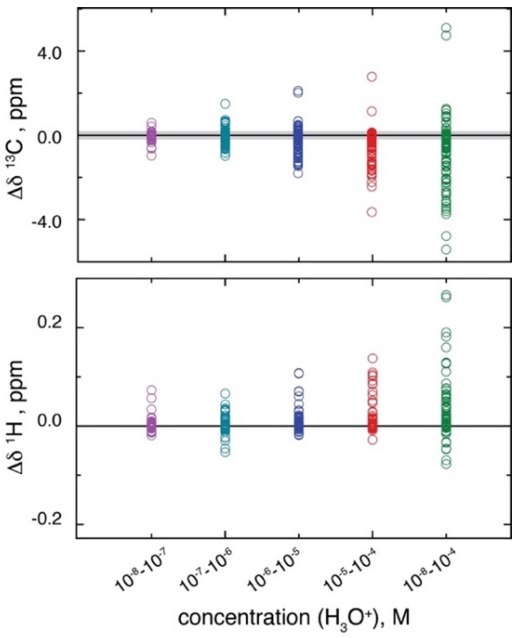

Fig. 2 Variation of ^{13}C (top) and ^{1}H (bottom) chemical shifts in all metabolites of Table 1 between 10^{-8} M and 10^{-4} M H_3O^+ (acidification from pH 8.0 to 4.0). The grey bar shows a region of ±0.2 ppm, an accuracy that has been considered achievable for ^{13}C NMR chemical shifts in inter-laboratory comparison with similar referencing.[44]

Table 1. ^{1}H and ^{13}C assignments of central metabolites relative to DSS at pH 4, 5, 6, 7 and 8 and 310 K

		pH 4.0		pH 5.0		pH 6.0		pH 7.0		pH 8.0	
		$\delta^{1}H$/ ppm	$\delta^{13}C$/ ppm	$\delta^{1}H$/ ppm	$\delta^{13}C$/ ppm	$\delta^{1}H$/ ppm	$\delta^{13}C$/ ppm	$\delta^{1}H$/ ppm	$\delta^{13}C$/ ppm	$\delta^{1}H$/ ppm	$\delta^{13}C$/ ppm
glycolysis and branching reactions:											
α-glucose	CH (1)	5.215	94.75	5.218	94.76	5.215	94.76	5.217	94.75	5.216	94.76
	CH (2)	3.518	74.18	3.521	74.19	3.517	74.19	3.519	74.19	3.520	74.22
	CH (3)	3.705	75.46	3.709	75.48	3.707	75.48	3.708	75.49	3.702	75.47
	CH (4)	3.459	72.37	3.396	72.35	3.394	72.35	3.395	72.35	3.395	72.34
	CH (5)	3.819	74.15	3.823	74.16	3.819	74.16	3.821	74.16	3.819	74.18
	CH_2 (6)	3.744; 3.826	63.33	3.747; 3.829	63.33	3.743; 3.826	63.32	3.745; 3.828	63.34	3.746; 3.828	63.34
β-glucose	CH (1)	4.627	98.61	4.630	98.61	4.626	98.60	4.628	98.60	4.629	98.62
	CH (2)	3.228	76.86	3.232	76.86	3.229	76.86	3.230	76.87	3.231	76.87
	CH (3)	3.447	78.63	3.451	78.65	3.448	78.65	3.449	78.65	3.449	78.65
	CH (4)	3.392	72.37	3.379	72.35	3.376	72.35	3.377	72.35	3.377	72.34
	CH (5)	3.479	78.49	3.483	78.49	3.479	78.49	3.481	78.49	3.482	78.48
	CH_2 (6)	3.706; 3.879	63.49	3.709; 3.882	63.48	3.705; 3.880	63.48	3.707; 3.881	63.48	3.707; 3.881	63.50
6-phosphogluconate	CO (1)		180.77		181.17		181.29		181.39		181.38
	CH (2)	4.147	76.38	4.148	76.67	4.145	76.74	4.157	76.80	4.157	76.82
	CH (3)	4.076	73.45	4.062	73.53	4.064	73.56	4.073	73.63	4.073	73.62
	CH (4)	3.866	72.89	3.863	72.91	3.844	73.09	3.809	73.45	3.800	73.46
	CH (5)	3.819	74.33	3.814	74.54	3.819	74.62	3.817	74.67	3.818	74.66
	CH_2 (6)	3.977; 4.081	68.95	3.972; 4.078	68.95	3.958; 4.047	68.62	3.937; 3.980	67.88	3.932; 3.971	67.76
α-glucose 6-	CH (1)	5.217	94.84	5.217	94.83	5.215	94.87	5.212	94.91	5.211	94.92
phosphate	CH (2)	3.545	74.19	3.550	74.17	3.551	74.25	3.557	74.34	3.559	74.38

	CH (3)	3.712	75.31	3.720	75.29	3.711	75.21	3.710	75.06	3.709	75.07
	CH (4)	3.506	71.93	3.506	71.92	3.518	71.93	3.572	71.85	3.583	71.85
	CH (5)	3.923	73.22	3.923	73.22	3.901	73.45	3.871	73.77	3.862	73.76
	CH_2 (6)	4.045; 4.067	66.68	3.962; 4.062	66.62	4.008; 4.056	66.22	3.920; 4.032	65.57	3.897; 4.023	65.43
β-glucose 6-	CH (1)	4.642	98.70	4.642	98.69	4.636	98.72	4.628	98.77	4.624	98.78
phosphate	CH (2)	3.257	76.84	3.260	76.83	3.265	76.91	3.267	76.99	3.269	77.06
	CH (3)	3.561	77.56	3.556	77.55	3.527	77.79	3.557	78.11	3.483	78.20
	CH (4)	3.489	71.93	3.492	71.92	3.502	71.93	3.548	71.85	3.558	71.85
	CH (5)	3.486	78.20	3.489	78.19	3.496	78.12	3.492	78.11	3.486	77.96
	CH_2 (6)	4.026; 4.122	66.71	4.030; 4.119	66.68	4.008; 4.056	66.22	3.9877; 4.104	65.66	3.976; 4.102	65.52
α-fructose 6-	CH_2 (1)	3.659; 3.627	65.58	3.652; 3.635	65.58	3.636; 3.652	65.58	3.6356; 3.6515	65.58	3.627; 3.662	65.63
phosphate	CO (2)		107.11		107.09		107.08		107.07		107.07
	CH (3)	4.139	82.62	4.137	82.68	4.130	82.88	4.113	83.19	4.114	83.27
	CH (4)	4.066	78.56	4.067	78.55	4.086	78.61	4.110	78.69	4.112	78.69
	CH (5)	4.102	84.63	4.100	84.60	4.091	84.57	4.083	84.55	4.084	84.55
	CH_2 (6)	4.058; 3.970	67.19	4.052; 3.962	67.11	3.924; 4.007	66.72	3.870; 3.939	66.16	3.867; 3.938	66.15
β-fructose 6-	CH_2 (1)	3.577; 3.539	65.46	3.576; 3.537	65.46	3.537; 3.576	65.46	3.537; 3.576	65.46	3.531; 3.571	65.50
phosphate	CO (2)		104.32		104.27		104.22		104.14		104.17
	CH (3)	4.108	77.96	4.108	77.99	4.102	78.02	4.099	78.06	4.093	78.09
	CH (4)	4.186	77.08	4.188	77.09	4.205	77.15	4.228	77.24	4.231	77.24
	CH (5)	3.916	82.06	3.914	82.06	3.907	82.33	3.894	82.68	3.894	82.71
	CH_2 (6)	4.039; 3.950	68.16	4.023; 3.946	68.07	3.908; 3.982	67.66	3.8595; 3.9151	67.02	3.856; 3.914	66.95
α-fructose 1,6-	CH_2 (1)	3.938; 3.914	68.23	3.900; 3.938	68.15	3.853; 3.833	67.72	3.799; 3.810	67.38	3.791; 3.955	67.35
bisphosphate	CO (2)		106.88		106.90		107.30		107.71		107.71
	CH (3)	4.099	84.30	4.093	84.31	4.074	84.29	4.062	84.22	4.060	84.22
	CH (4)	4.073	78.83	4.071	78.89	4.064	79.13	4.043	79.64	4.037	79.72
	CH (5)	4.178	83.58	4.175	83.66	4.170	84.05	4.170	84.88	4.169	84.83

	CH_2 (6)	3.976; 4.037	67.58	3.968; 4.031	67.57	3.934; 3.990	67.43	3.940; 3.963	67.37	3.861; 3.906	66.95
β-fructose 1,6-bisphosphate	CH_2 (1)	3.815; 3.864	68.58	3.813; 3.855	68.56	3.790; 3.822	68.55	3.749; 3.784	68.57	3.771; 3.841	68.55
	CO (2)		103.34		103.35		103.56		103.70		103.68
	CH (3)	4.172	78.27	4.171	78.31	4.169	78.50	4.159	78.69	4.159	78.73
	CH (4)	4.187	76.82	4.172	76.83	4.174	76.93	4.186	77.06	4.184	77.07
	CH (5)	3.949	81.97	3.946	82.01	3.930	82.13	3.913	82.41	3.910	82.41
	CH_2 (6)	3.953; 4.035	67.94	3.951; 4.029	67.92	3.924; 3.986	67.63	3.873; 3.915	67.06	3.861; 3.906	67.02
glyceraldehyde 3-phosphate, hydrate	CO (1)	4.991	92.10	4.991	92.10	4.993	92.27	4.995	92.58	4.994	92.61
	CH (2)	3.696	75.74	3.693	75.75	3.677	75.93	3.644	76.17	3.646	76.22
	CH_2OP (3)	3.906; 4.002	68.39	3.905; 4.000	68.32	3.886; 3.967	67.88	3.851; 3.916	67.24	3.851; 3.907	67.19
dihydroxyacetone phosphate	CH_2OP (1)	4.592	70.49	4.574	70.46	4.503	70.25	4.467	70.15	4.464	70.16
	CO (2)		212.15		212.28		213.74		214.34		214.38
	CH_2OH (3)	4.504	67.95	4.508	67.97	4.525	68.05	4.534	68.10	4.535	68.11
dihydroxyacetone phosphate, hydrate	CH_2OP (1)	3.846	69.35	3.838	69.26	3.806	68.93	3.794	68.74	3.795	68.75
	CO (2)		97.12		97.23		97.43		97.62		97.67
	CH_2OH (3)	3.575	66.47	3.567	66.50	3.549	66.70	3.541	66.85	3.544	66.86
glycerol	CH_2 (1)	3.548; 3.636	65.26	3.547; 3.637	65.25	3.547; 3.636	65.25	3.546; 3.636	65.24	3.550; 3.638	65.26
	CH (2)	3.765	74.74	3.767	74.78	3.765	74.77	3.768	74.77	3.767	74.76
2,3-bisphospho-glycerate	CO (1)		178.31		178.78		179.02		180.00		180.96
	CH (2)	4.623	78.07	4.594	78.35	4.582	78.44	4.551	78.32	4.494	77.72
	CH_2 (3)	4.115; 4.140	69.48	4.099; 4.138	69.59	4.077; 4.127	69.52	4.019; 4.088	69.31	4.001; 4.055	69.12
3-phosphoglycerate	CO (1)		180.15		180.51		180.74		181.35		181.39
	CH (2)	4.237	74.67	4.189	74.94	4.179	75.15	4.166	75.70	4.164	75.80
	CH_2 (3)	4.001; 4.104	70.29	3.972; 4.091	70.42	3.946; 4.074	70.24	3.860; 4.020	69.57	3.844; 4.014	69.45
2-phosphoglycerate	CO (1)		179.05		179.38		179.66		180.49		180.74
	CH (2)	4.517	79.54	4.489	79.82	4.483	79.69	4.465	79.08	4.460	78.93
	CH_2 (3)	3.843; 3.881	66.30	3.830; 3.873	66.46	3.817; 3.874	66.70	3.782; 3.883	67.35	3.7734; 3.8849	67.59

Please do not adjust margins

phosphoenolpyruvate	CO (1)		172.52		173.11		174.01		174.62		174.62
	=COP (2)		151.17		151.74		152.29		152.60		152.62
	$=CH_2$ (3)	5.288; 5.584	107.22	5.239; 5.516	106.12	5.197; 5.412	104.05	5.168; 5.335	102.55	5.1665; 5.3323	102.48
pyruvate	CO (1)		173.03		173.00		173.01		173.01		173.08
	CO (2)		207.88		207.92		207.94		207.94		207.98
	CH_3 (3)	2.355	29.09	2.359	29.13	2.342	28.90	2.342	28.92	2.355	29.10
pyruvate, hydrate	CO (1)		180.77		181.16		181.16		181.16		181.24
	OCO (2)		96.43		96.54		96.53		96.54		96.62
	CH_3 (3)	1.477	27.81	1.474	27.83	1.473	27.85	1.473	27.85	1.469	27.82
alanine	CO (1)		178.41		178.40		178.39		178.38		178.59
	CH (2)	3.773	53.24	3.770	53.24	3.770	53.25	3.770	53.25	3.761	53.27
	CH_3 (3)	1.467	18.80	1.467	18.81	1.466	18.81	1.467	18.81	1.462	18.90
lactate	CO (1)		184.28		184.93		185.03		185.07		185.05
	CH (2)	4.147	70.81	4.100	71.13	4.090	71.20	4.090	71.21	4.089	71.21
	CH_3 (3)	1.332	22.59	1.317	22.74	1.313	22.76	1.314	22.77	1.313	22.78
acetaldehyde	CO (1)	9.667	209.52	9.666	209.54	9.667	209.52	9.670	209.55	9.670	209.54
	CH_3 (2)	2.228	32.84	2.228	32.83	2.228	32.83	2.229	32.83	2.229	32.84
acetaldehyde, hydrate	OCO (1)	5.228	90.90	5.229	90.89	5.228	90.89	5.228	90.90	5.231	90.91
	CH_3 (2)	1.318	25.83	1.317	25.80	1.317	25.80	1.318	25.83	1.317	25.82
acetate	CO (1)		180.83		183.09		183.95		184.06		184.07
	CH_3 (2)	2.028	23.96	1.936	25.40	1.903	25.93	1.900	25.98	1.899	25.99
ethanol	CH_2 (1)	3.637	60.13	3.638	60.12	3.638	60.12	3.638	60.12	3.638	60.12
	CH_3 (2)	1.169	19.50	1.169	19.50	1.169	19.50	1.169	19.50	1.168	19.53
formate	CH	8.411	172.82	8.439	173.60	8.443	173.63	8.445	173.62	8.444	173.64
α, α-trehalose	CH (1)	5.179	95.96	5.180	95.97	5.181	95.91	5.181	95.95	5.180	95.96
	CH (2)	3.635	73.77	3.634	73.77	3.634	73.76	3.637	73.76	3.633	73.78
	CH (3)	3.837	75.27	3.837	75.28	3.837	75.22	3.842	75.26	3.839	75.26
	CH (4)	3.438	72.41	3.438	72.44	3.435	72.39	3.442	72.42	3.438	72.41
	CH (5)	3.814	74.87	3.815	74.88	3.811	74.82	3.816	74.87	3.815	74.89
	CH_2 (6)	3.746; 3.846	63.26	3.747; 3.846	63.28	3.748; 3.846	63.21	3.750; 3.849	63.27	3.748; 3.846	63.26

citric acid cycle and branching reactions:											
citrate	CO (1)		178.40		179.92		181.41		181.97		182.00
	CH_2 (2)	2.730; 2.827	46.73	2.657; 2.739	47.39	2.565; 2.665	48.14	2.521; 2.647	48.44	2.519; 2.642	48.45
	COH (3)		77.24		77.24		77.67		77.82		77.84
	CO (sc)[§]		181.84		182.92		184.20		184.57		184.59
isocitrate	CO (1)		180.79		180.97		182.47		182.88		182.92
	CHOH (2)	4.220	75.14	4.119	75.76	4.011	76.21	3.945	76.39	3.958	76.44
	CH (3)	3.221	49.34	3.113	50.23	3.006	51.24	2.962	51.70	2.954	51.76
	CH_2 (4)	2.586; 2.707	37.05	2.505; 2.620	38.41	2.438; 2.534	39.74	2.413; 2.498	40.35	2.408; 2.497	40.43
	CO (5)		180.53		181.83		182.87		183.53		183.68
	CO (sc)		179.66		183.34		184.72		185.02		185.07
α-ketoglutarate	CO (1)		172.75		172.87		172.86		172.86		172.79
	CO (2)		207.73		209.00		208.22		208.37		208.41
	CH_2 (3)	2.993	37.29	2.972	38.03	2.974	38.42	2.971	38.48	2.989	38.57
	CH_2 (4)	2.608	31.26	2.471	32.67	2.426	33.25	2.422	33.33	2.426	33.35
	CO (5)		181.26		183.16		183.87		183.96		183.98
succinate	CO (1)		181.54		183.40		184.80		185.03		185.02
	CH_2 (2)	2.576	33.19	2.472	35.19	2.402	36.66	2.388	36.96	2.385	36.93
fumarate	CO (1)		175.79		177.06		177.30		177.29		177.31
	CH (2)	6.591	137.67	6.521	137.97	6.506	137.99	6.505	137.99	6.504	137.98
malate	CO (1)		179.69		181.42		182.35		182.45		182.45
	CHOH (2)	4.353	71.64	4.301	72.58	4.284	73.05	4.281	73.10	4.276	73.10
	CH_2 (3)	2.585; 2.790	43.23	2.431; 2.703	44.63	2.358; 2.660	45.30	2.347; 2.656	45.37	2.362; 2.652	45.30
	CO (4)		182.17		183.09		183.52		183.60		183.59
oxaloacetate	CO (1)		171.15		171.19		171.35		171.31		171.30
	CO (2)		202.87		203.06		203.25		203.20		203.29
	CH_2 (3)	3.639	51.43	3.631	51.55	3.630	51.56	3.632	51.55	3.634	51.55
	CO (4)		176.89		177.19		177.32		177.28		177.27
glutamate	CO (1)		176.87		177.08		177.10		177.27		177.28
	CH (2)	3.762	57.07	3.744	57.39	3.739	57.44	3.735	57.45	3.724	57.45
	CH_2 (3)	2.083; 2.137	28.94	2.050; 2.123	29.50	2.039; 2.118	29.61	2.026; 2.115	29.67	2.029; 2.110	29.73

Please do not adjust margins

	CH_2 (4)	2.450	34.52	2.365	35.95	2.345	36.26	2.343	36.28	2.339	36.29
	CO (5)		181.82		183.52		183.93		183.95		183.94
glutamine	CO (1)		176.47		176.56		176.56		176.66		177.28
	CH (2)	3.764	56.89	3.762	56.90	3.761	56.90	3.756	56.90	3.721	56.99
	CH_2 (3)	2.128	28.85	2.128	28.85	2.128	28.85	2.124	28.91	2.106	29.24
	CH_2 (4)	2.450	33.56	2.445	33.59	2.445	33.59	2.450	33.58	2.434	33.61
	CO (5)		180.33		180.31		180.32		180.31		180.49
itaconate	CO (1)		180.45		181.87		183.00		183.26		183.30
	C= (2)		139.87		142.34		144.18		144.62		144.64
	CH_2 (3)	3.302	42.43	3.216	43.69	3.155	44.51	3.140	44.68	3.141	44.68
	CO (4)		175.47		177.12		178.26		178.53		178.58
	$=CH_2$ (sc)	5.649; 6.106	129.47	5.492; 5.954	126.73	5.385; 5.859	124.75	5.359; 5.836	124.28	5.360; 5.835	124.37
detoxification route for acetaldehyde:											
acetoin	CH_3 (1)	2.214	27.65	2.214	27.65	2.213	27.64	2.213	27.64	2.214	27.64
	CO (2)		218.27		218.28		218.24		218.29		218.31
	CH (3)	4.400	75.73	4.401	75.73	4.398	75.72	4.399	75.72	4.399	75.72
	CH_3 (4)	1.360	20.94	1.362	20.92	1.361	20.94	1.360	20.94	1.362	20.93
meso 2,3-butanediol	CH (1)	3.704	73.72	3.703	73.73	3.700	73.70	3.704	73.71	3.704	73.71
	CH_3 (2)	1.127	19.44	1.129	19.44	1.126	19.41	1.128	19.40	1.128	19.41
racem 2,3-butanediol	CH (1)	3.607	74.20	3.606	74.18	3.606	74.18	3.606	74.18	3.608	74.19
	CH_3 (2)	1.129	20.36	1.126	20.33	1.126	20.33	1.129	20.33	1.129	20.35

[§]sc indicates branches deviating from a linear carbon backbone

Considering the strong variation of metabolite chemical shifts at hydronium concentrations between 10^{-4} M and 10^{-8} M (pH 4.0-8.0), we finally evaluated, if alkali ion concentrations in the physiological range likewise have a significant effect on the ^{13}C chemical shifts. Use of KCl in concentrations of up to 400 mM at pH 7.0 and 310 K did not significantly impact ^{13}C chemical shifts of selected metabolites such as citrate and succinate (Fig. S4, S5) that had exhibited pH dependent of up to above 3 ppm for hydronium concentrations of up to 0.1 mM (pH 4.0; Table 1). In contrast to hydronium concentrations, alkali ion concentrations thus had a minor effect on ^{13}C chemical shifts, while it had been shown previously that temperature variation near physiological values likewise has a very minor impact on ^{13}C chemical shifts.[11]

3.2 D-DNP assay of upper glycolysis in PC-3 cancer cells

Motivated by the predictable correlation between hydronium concentrations and chemical shifts for various functional groups, and considering the negligible effects of alkali ions, we pursued the unambiguous identification of metabolites in upper glycolysis by a cancer cell line (prostate cancer cell line PC-3).

3.2.1 Identification of accumulating intermediates

Initial bottlenecks in D-[1-^{13}C,1-^{2}H]glucose conversion were assessed by hyperpolarization using dissolution dynamic nuclear polarization (D-DNP) NMR spectroscopy. Embden-Meyerhof-Parnas (EMP) glycolysis in cancer cells is known to be affected through the 'Warburg effect' and may be a prospective target for cancer treatment. D-DNP-NMR had shown promise in evaluating glucose uptake and glycolytic flux through enzymatic steps and entire pathways in cells using D-[U-^{13}C,U-^{2}H]glucose.[48–50] Such D-DNP-NMR assays can also provide information on the cellular redox state.[30]

As D-DNP operates on a timescale of seconds to minutes, only a minor part of the spin-polarization enhanced substrate is converted during this time span.[31,48] Hence, background from the D-[U-^{13}C,U-^{2}H]glucose substrate obscures most metabolites in the upper part of glycolysis, which are carbohydrates like glucose itself. Accordingly, D-DNP using carbohydrate substrates[31,50–55] had proven more promising in identifying bottlenecks downstream of fructose-1,6 bisphosphate with characteristic quaternary carbons such as dihydroxyacetone phosphate, 3-phosphoglycerate, and pyruvate.[31,48,56]

We hypothesized that the commercially available D-[1-^{13}C,1-^{2}H]glucose may be a suitable substrate to render intermediates in upper glycolysis detectable. D-DNP enhanced D-[1-^{13}C,1-^{2}H]glucose fulfils a double role in strides to characterize cancer metabolism. Firstly, the absence of deuterated and ^{13}C-enriched alcoholic groups at C2-C5 should render the initial steps in the conversion of D-[1-^{13}C,1-^{2}H]glucose detectable, as products of glucose and glucose-6-phosphate are alcohol and phosphoester groups devoid of a C1 hemiacetal group (Figure 3A), resulting in significantly different ^{13}C chemical shifts of strong substrate signal and metabolites in upper glycolysis. Secondly, the site specific isotope labelling can afford a more detailed mechanistic tracking than D-[U-^{13}C,U-^{2}H]glucose by clarifying the fate of the C1 carbon.[57]

Fig. 3B shows the ^{13}C NMR spectral region containing free primary alcohol groups and phosphoesters to primary alcohols obtained applying a bolus of D-[1-^{13}C,1-^{2}H]glucose to a cell suspension of PC-3. In this assay, 0.33 mL hyperpolarized D-[1-^{13}C,1-^{2}H] glucose (10 mM) were manually injected into 0.2 mL, resulting in a final concentration of 6.2 mM hyperpolarized D-[1-^{13}C,1-^{2}H] glucose. As anticipated, the detection of signals in the alcohol region of the spectrum became possible, when using D[1-^{13}C,1-^{2}H]glucose as the D-DNP substrate. Due to fast D-DNP assay timescale, the prospect to acquire assignment spectra to identify transient signals by assignment spectra is limited. Hence, signal identification using D-DNP enhancement and NMR detection usually relies on the use of suitable reference compounds. Identification of the metabolite signals deriving from D-[1-^{13}C,1-^{2}H]glucose indicated challenges when relying on NMR databases and literature data. In contrast to the identification of signals for lactate, pyruvate, 6-phosphogluconate and CO_2/HCO_3^- in the ^{13}C chemical shift range 20-182 ppm (Fig. S6), the unambiguous identification of

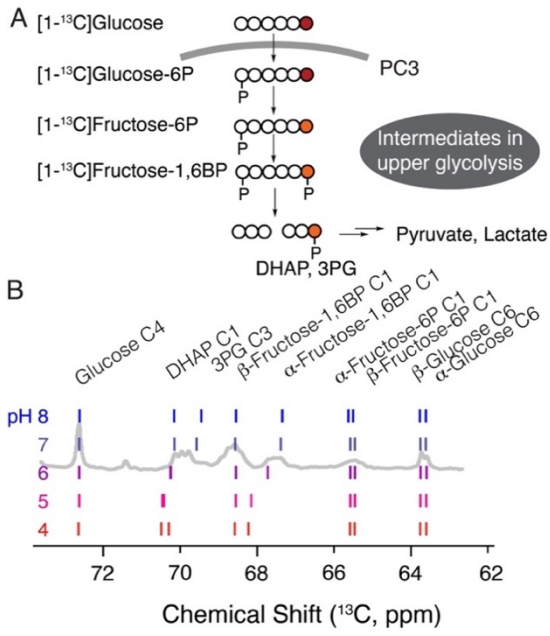

Fig. 3 (A) D-DNP assay using hyperpolarized D-[1-^{13}C,1-^{2}H]glucose to probe the conversion of glucose to intermediates of upper glycolysis. The site-specific label serves to avoid overlap with glucose substrate, while pH dependent reference data allow identification of different metabolites in a narrow chemical shift range: upper glycolysis mostly converts the C1 position of glucose (red) to primary alcohol groups and their phosphoesters (orange). (B) The pH dependence of chemical shifts for products of D-[1-^{13}C,1-^{2}H]glucose in EMP glycolysis allows concurrent identification of signals and determination of intracellular pH. Abbreviations: 3PG: 3-phosphoglycerate, DHAP: dihydroxyacetone phosphate.

signals between 60-70 ppm for intracellular intermediates of upper glycolysis from D-[1-^{13}C,1-^{2}H]glucose posed a greater challenge, which could be solved by the data of Table 1 to yield the assignments shown in Figure 3B through comparison with pH dependent signal positions.

3.2.2 Deviation from reference data identifies useful reporters of intracellular pH

The titration of the phosphate group near physiological pH has been recognized as a means to probe intracellular pH based on chemical shift assignments near neutral pH. Due to the distinct pH dependence of ^{13}C chemical shifts for the metabolites of upper glycolysis, the pattern of chemical shifts was indicative of the intracellular pH. Fig. 3B compares the ^{13}C chemical shifts of metabolites of upper glycolysis at five different pH values between 4.0 and 8.0 with the observed D-DNP spectrum. These metabolites maintain one deuterium attached to the phosphorylated site deriving from glucose C1. A chemical shift correction of 0.36 ppm due to deuteration was applied in the referencing of the experimental data.[59] The chemical shift pattern of reference compounds as shown in Fig.3B indicated that the pH dependence of ^{13}C NMR chemical shifts for metabolites of upper glycolysis is useful for probing intracellular pH, providing a pH-dependent "barcode" of ^{13}C NMR chemical shifts. This pH dependence also allowed unambiguous identification of signals without perfect chemical shift agreement to tabulated data, as intracellular signals for 3-phosphoglycerate and of α-fructose-1,6-bisphosphate both were found to appear at chemical shift values between those expected at pH 6.0 and 7.0 (Fig. 3B).

The comparison of pH-dependent reference data and of in-cell data further showed that some sites (such as β-fructose-1,6-bisphosphate C1) exhibit pH-invariant ^{13}C chemical shifts and can serve as prospective internal reference sites for chemical shift calibration (Figure 3B). Intracellular NMR signals for these compounds yielded excellent agreement with reference data at pH 7.0 within the experimental error of chemical shift determinations, as shown in Fig. 4A,B. This correlation indicated that intracellular chemical shifts were determined with an accuracy below 0.2 ppm. Exceptions were the metabolites whose chemical shifts depend most strongly on pH near physiological conditions, specifically 3-phosphoglycerate (C3 position) and to a lesser degree the α-anomer of fructose-1,6-bisphosphate (C1 position). The observed intracellular ^{13}C chemical shifts indicated that the cytosolic pH in PC-3 cells following the glucose bolus (6.2 mM) was 6.5±0.1. Hence, ^{13}C chemical shifts for metabolites formed from hyperpolarized D-[1-^{13}C,1-^{2}H]glucose in upper glycolysis provide an alternative approach to non-invasive measurements of pH in cancer cells, which has previously been pursued by conventional ^{31}P NMR[45] and by D-DNP NMR using the physiological bicarbonate buffer.[60]

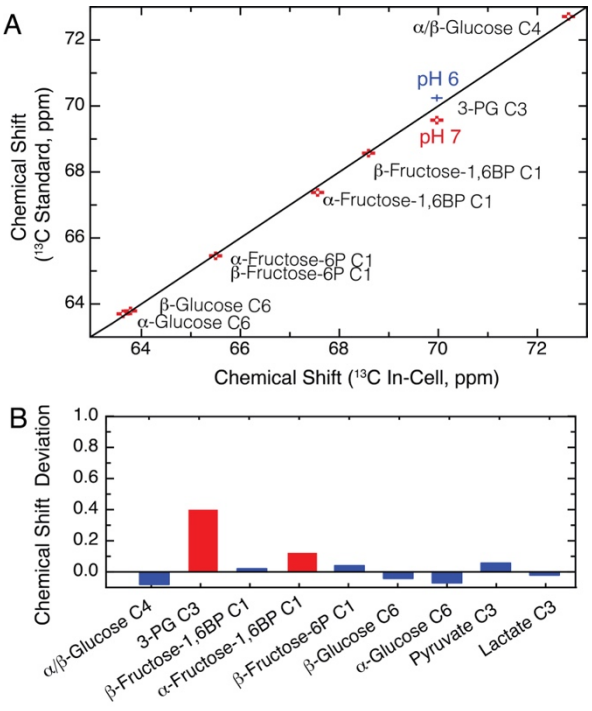

Fig. 4 (A) Correlation between intracellular metabolite chemical shifts and chemical shifts expected from reference compounds at pH 7.0. Deviations from expected values at pH7.0 are shown in (B) and can be ascribed to an intracellular pH between 6.0 and 7.0.

3.3 Ability to follow oxidative part of the PPP in cancer cells in the presence of adjuvant

Following the detection of upper glycolysis and intracellular pH in PC-3 cell lines based on pH dependent reference data and site-specific isotope labelling, we finally evaluated, if additional pathways of glucose usage can be probed using hyperpolarized D-DNP NMR. To this end, the influx of hyperpolarized D-[1-13C,1-2H]glucose into PC-3 metabolism was compared in the absence and in the presence of exogeneous pyruvate.

Diversion of cytoplasmic glucose to PPP, which provides building blocks to proliferating cells, has been related to tumor metastasis in prostate cancer.[61–63] A better understanding of the regulation of glucose metabolism in cancer is still needed for combating cancer through metabolic inhibitors.[47] While the C1 site of hyperpolarized D-[1-^{13}C,1-^{2}H]glucose forms primary alcohol groups and their phosphoesters in upper glycolysis, other oxidation states are formed in lower EMP glycolysis and the oxidative part of the PPP (Scheme 2A). Isotope enriched $^{13}CO_2$ is liberated from the glucose ^{13}C1 position in the pentose phosphate pathway (PPP), while the glucose ^{13}C1 position forms the methyl group in pyruvate and lactate.[48] Hence, the fate of the glucose C1 position is easily identified due to characteristic chemical shifts of the products in lower glycolysis and the PPP.

We hypothesized that D-DNP observations of cancer metabolism using D-[1-^{13}C,1-^{2}H]glucose substrate may be further optimized by the presence of an adjuvant to modulate uptake or metabolism. Covalent modification of substrates and pretreatment of cells have previously been employed for improved substrate uptake.[5,64–66] In addition, unlabeled lactate

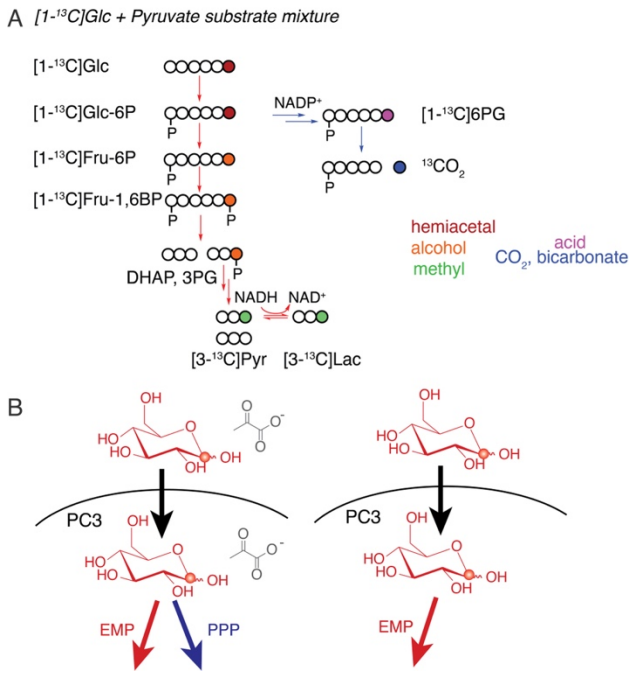

Scheme 2 Probing PC-3 metabolism with a mixture of hyperpolarized [1-^{13}C,1-^{2}H]glucose and non-detected pyruvate adjuvant. (A) The C1 position in glucose experiences transformation between various oxidation states and hence significant chemical shift changes, not least for metabolites from the PPP. (B) Schematic overview over the probing of PC-3 metabolism using hyperpolarized [1-^{13}C,1-^{2}H]glucose as the metabolic probe molecule in the presence (left) and in the absence (right) of pyruvate, which has been implicated in the proliferation of cancer cells. Abbreviations: 3PG: 3-phosphoglycerate, 6PG: 6-phosphogluconate, DHAP: dihydroxyacetone phosphate, EMP: Embden Meyerhof Parnas pathway, Fru: fructose, Glc: glucose, Lac: lactate, PPP: pentose phosphate pathway, Pyr: pyruvate.

has been used to enhance [1-^{13}C]lactate signal derived from [1-^{13}C]pyruvate by increasing pool sizes and stimulating exchange.[29,52]

Pyruvate has been shown to promote the proliferation of multiple cancer cell types, including pancreatic cancer.[26–28] Hence, insight into the metabolism of glucose/pyruvate mixtures by PC-3 cells may aid in clarifying the metabolic effect of persistent exogeneous pyruvate, which is secreted for instance by cancer-associated fibroblasts in the pancreas and elicits a redox-dependent effect in tumors that depends on pyruvate to lactate conversion.[28] Pyruvate is a more oxidized substrate than glucose and is in rapid reversible exchange with lactate in most cancer cells.[29] We therefore conjectured that the presence of pyruvate adjuvant may make effects on glucose metabolism in cancer cells detectable by D-DNP. Pyruvate addition could be expected to affect the cellular redox state, possibly including a more facile influx of glucose into the initial, oxidative branch of the PPP.

The comparison of PC-3 metabolism as probed by D-DNP NMR is displayed in Fig.5 in the absence (blue) and in the presence (red) of pyruvate adjuvant (at 20 mM final concentration). This comparison showed that the presence of pyruvate as a non-labelled adjuvant provided with the hyperpolarized substrate indeed allowed detection of C1-labelled 6-phosphogluconate and its decarboxylation to CO_2 and bicarbonate in the PPP detectable (red spectrum in Fig. 5, time course data of the experiment shown in Fig. S6). By

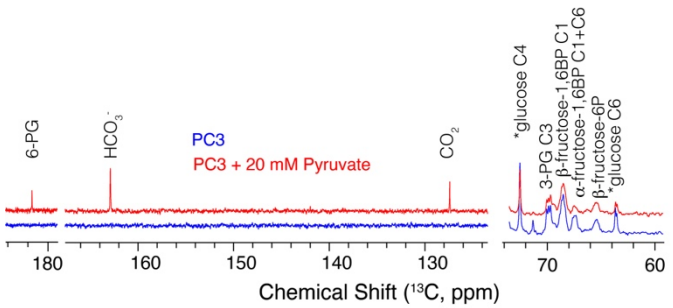

Fig. 5 Projection of 50 1D ^{13}C NMR spectra acquired within 25 seconds after the injection of hyperpolarized D-[1-^{13}C,1-^{2}H]glucose to PC-3 cancer cells (40 mM phosphate buffer, pH 7.4) in the absence (blue) and in the presence of 20 mM pyruvate. The presence of pyruvate renders influx of glucose into the pentose phosphate pathway visible through 6-phosphogluconate and CO_2/HCO_3^- signal. Spectra are normalized to identical glucose C1 signals.

contrast, D-DNP using hyperpolarized D-[1-^{13}C,1-^{2}H]glucose substrate alone (blue spectrum in Fig. 5) did not reveal any formation of CO_2 or yield other indication of PPP activity. These observations showed that the scope of tracers for in-cell observations can be diversified by the presence of adjuvants to probe additional pathways. More importantly, the results indicated that the recently proposed effect of pyruvate on proliferation of cancer cells is paralleled by some diversion of glucose from the EMP to the PPP (Scheme 2), which produces building blocks for proliferation. It seems likely that rerouting upon addition of exogeneous pyruvate is not the consequence of an inhibition of EMP glycolysis, as activity of glycolysis and of pyruvate metabolism in cancer cells have previously been shown to be positively correlated.[67] Signals for the alcohols of upper glycolysis (60-70 ppm) were only little affected in intensity and signal position by the presence of 20 mM adjuvant pyruvate (Fig. 5). This similarity indicates that the bottlenecks of upper EMP glycolysis were not significantly affected by the adjuvant and that altered glucose usage in the presence of adjuvant did not derive from an effect of the adjuvant on intracellular pH.

Flux of hyperpolarized D-[1-^{13}C,1-^{2}H]glucose through the entire glycolytic pathway to lactate could be traced within less than 30 seconds of NMR experiment time, both in the absence and in the presence of exogeneous pyruvate (Fig. S7). This observation is noteworthy, as the C1 position in D-[1-^{13}C,1-^{2}H]glucose is protonated upon conversion of glucose-6-phosphate to its ketohexose isomer fructose-6-phosphate, while a second hydrogen is incorporated in the conversion of phosphoenolpyruvate to pyruvate. Hydrogen incorporation at C1 in D-[1-^{13}C,1-^{2}H]glucose elicits a significant shortening of the T_1 time, and the detection of hyperpolarized C1 flux through the entire glycolysis hence underlines the ability for rapid conversion of glucose to lactate on the low seconds timescale. These observations indicate that D-DNP methodology using hyperpolarized D-[1-^{13}C,1-^{2}H]glucose in the absence and presence of additives can play a role in elucidating the interplay between glycolysis, PPP and fermentation in tumor environments.

4. Conclusions

In conclusion, we have pursued a systematic approach to identify and address limitations in the observation of intracellular metabolism by NMR spectroscopy, with an emphasis on D-DNP NMR spectroscopy. Due to poor *a priori* knowledge and lacking control of intracellular pH, a collection of pH dependent metabolite signals was obtained in the physiological pH range of 4.0-8.0. Unambiguous identifications of intracellular metabolites with chemically similar sites, such as the primary alcohol groups deriving from the C1 glucose position, were viable using an extensive compendium of pH-dependent chemical shift assignments. This compendium should facilitate increasingly detailed mechanistic insights into central metabolism in biomedically relevant cells and other samples, whose pH is impossible or cumbersome to control. Here, the reference collection allowed the concurrent intracellular pH determination and identification of accumulating intermediates in upper glycolysis in measurements employing hyperpolarized D-[1-^{13}C,1-^{2}H]glucose to probe PC-3 metabolism. The site-specific labelling in the substrate affords the detection of metabolites in upper glycolysis by avoiding overlap with substrate signals.

In addition to reduced overlap with the substrate, the site-specific labelling allowed the distinction of glucose influx into EMP glycolysis and into the PPP. The detection of metabolites of lower glycolysis, which are indicative of cellular redox state, was still possible using hyperpolarized D-[1-^{13}C,1-^{2}H]glucose in PC-3. Glucose influx into PC-3 metabolism was compared in the absence and in the presence of exogeneous pyruvate. Pyruvate, which can be secreted by cells near the cancer, had been shown to promote the proliferation of cancer cells. Influx of hyperpolarized D-[1-^{13}C,1-^{2}H]glucose into PC-3 metabolism indicated that this effect of pyruvate on proliferation of cancer cells is reflected by an activation of influx into the oxidative part of the PPP, which provides building blocks for proliferation. From an analytical perspective, suitable adjuvants can improve the scope of hyperpolarized substrates for D-DNP NMR by rendering additional intracellular conversions detectable.

Author Contributions

PRJ, SM: conceptualization, methodology, supervision; KCW, PRJ: cell culture, hyperpolarization; PRJ, SM: D-DNP NMR; FS: reference spectra collection, assignment, deposition; FS, PRJ, SM: data analysis; SM: figures and writing original draft; all authors: reviewing and editing of manuscript. All authors have read and approved the final version of the manuscript.

Conflicts of interest

There are no conflicts to declare.

Acknowledgement

The authors gratefully acknowledge support by the Independent Research Fund Denmark (Green transition programme, grant 0217-00277A). 800 MHz NMR spectra NMR spectra were recorded at the NMR Center DTU, supported by the Villum Foundation. D-DNP NMR data were acquired with equipment partially funded by the Novo Nordisk Foundation (NNF 19OC0055825).

Notes and references

1 A. Stincone, A. Prigione, T. Cramer, M. M. C. Wamelink, K. Campbell, E. Cheung, V. Olin-Sandoval, N.-M. Grüning, A. Krüger, M. Tauqeer Alam, M. A. Keller, M. Breitenbach, K. M. Brindle, J. D. Rabinowitz and M. Ralser, *Biol. Rev. Camb. Philos. Soc.*, 2015, **90**, 927–963.
2 G. A. Nagana Gowda and D. Raftery, *Anal. Chem.*, 2023, **95**, 83–99.
3 R. Dubey, N. Sinha and N. R. Jagannathan, *NMR Biomed.*, , DOI:10.1002/nbm.4686.
4 I. Martínez-Reyes and N. S. Chandel, *Nat. Rev. Cancer*, 2021, **21**, 669–680.
5 S. Meier, P. Jensen, M. Karlsson and M. Lerche, *Sensors*, 2014, **14**, 1576–1597.
6 K. R. Keshari and D. M. Wilson, *Chem Soc Rev*, 2014, **43**, 1627–1659.
7 N. J. Stewart, T. Sato, N. Takeda, H. Hirata and S. Matsumoto, *Antioxid. Redox Signal.*, 2022, **36**, 81–94.
8 T. Cheng, A. P. Gaunt, I. Marco-Rius, M. Gehrung, A. P. Chen, J. J. van der Klink and A. Comment, *NMR Biomed.*, 2020, **33**, e4264.
9 H. Kovacs, D. Moskau and M. Spraul, *Prog. Nucl. Magn. Reson. Spectrosc.*, 2005, **46**, 131–155.
10 J. J. Ellinger, R. A. Chylla, E. L. Ulrich and J. L. Markley, *Curr. Metabolomics*, 2013, **1**, 28–40.
11 F. Sannelli, P. R. Jensen and S. Meier, *Anal. Chem.*
12 E. Luchinat, M. Cremonini and L. Banci, *Chem. Rev.*, 2022, **122**, 9267–9306.
13 I. H. Madshus, *Biochem. J.*, 1988, **250**, 1–8.
14 V. P. Chacko and R. G. Weiss, *Am. J. Physiol.-Cell Physiol.*, 1993, **264**, C755–C760.
15 B. Yang, C. Zhang, S. Cheng, G. Li, J. Griebel and J. Neuhaus, *Diagnostics*, 2021, **11**, 149.
16 S. Tiziani, V. Lopes and U. L. Günther, *Neoplasia*, 2009, **11**, 269-IN10.
17 G. D. Tredwell, J. G. Bundy, M. De Iorio and T. M. D. Ebbels, *Metabolomics*, 2016, **12**, 152.
18 A. M. Weljie, J. Newton, P. Mercier, E. Carlson and C. M. Slupsky, *Anal. Chem.*, 2006, **78**, 4430–4442.
19 K. Golman, R. in't Zandt, M. Lerche, R. Pehrson and J. H. Ardenkjaer-Larsen, *Cancer Res.*, 2006, **66**, 10855–10860.
20 A. Dey, B. Charrier, E. Martineau, C. Deborde, E. Gandriau, A. Moing, D. Jacob, D. Eshchenko, M. Schnell, R. Melzi, D. Kurzbach, M. Ceillier, Q. Chappuis, S. F. Cousin, J. G. Kempf, S. Jannin, J.-N. Dumez and P. Giraudeau, *Anal. Chem.*, 2020, **92**, 14867–14871.
21 C. S. Clendinen, B. Lee-McMullen, C. M. Williams, G. S. Stupp, K. Vandenborne, D. A. Hahn, G. A. Walter and A. S. Edison, *Anal. Chem.*, 2014, **86**, 9242–9250.

22 J. H. Ardenkjaer-Larsen, B. Fridlund, A. Gram, G. Hansson, L. Hansson, M. H. Lerche, R. Servin, M. Thaning and K. Golman, *Proc. Natl. Acad. Sci. U. S. A.*, 2003, **100**, 10158–10163.
23 J.-H. Ardenkjaer-Larsen, G. S. Boebinger, A. Comment, S. Duckett, A. S. Edison, F. Engelke, C. Griesinger, R. G. Griffin, C. Hilty, H. Maeda, G. Parigi, T. Prisner, E. Ravera, J. van Bentum, S. Vega, A. Webb, C. Luchinat, H. Schwalbe and L. Frydman, *Angew. Chem. Int. Ed.*, 2015, **54**, 9162–9185.
24 M. Karlsson, P. R. Jensen, J. Ø. Duus, S. Meier and M. H. Lerche, *Appl. Magn. Reson.*, 2012, **43**, 223–236.
25 A. Comment and M. E. Merritt, *Biochemistry*, 2014, **53**, 7333–7357.
26 R. Datta, S. Sivanand, A. N. Lau, L. V. Florek, A. M. Barbeau, J. Wyckoff, M. C. Skala and M. G. Vander Heiden, *Sci. Adv.*, 2022, **8**, eabg6383.
27 A. Luengo, Z. Li, D. Y. Gui, L. B. Sullivan, M. Zagorulya, B. T. Do, R. Ferreira, A. Naamati, A. Ali, C. A. Lewis, C. J. Thomas, S. Spranger, N. J. Matheson and M. G. Vander Heiden, *Mol. Cell*, 2021, **81**, 691-707.e6.
28 S. A. Kerk, L. Lin, A. L. Myers, D. J. Sutton, A. Andren, P. Sajjakulnukit, L. Zhang, Y. Zhang, J. A. Jiménez, B. S. Nelson, B. Chen, A. Robinson, G. Thurston, S. B. Kemp, N. G. Steele, M. T. Hoffman, H.-J. Wen, D. Long, S. E. Ackenhusen, J. Ramos, X. Gao, Z. C. Nwosu, S. Galban, C. J. Halbrook, D. B. Lombard, D. R. Piwnica-Worms, H. Ying, M. Pasca Di Magliano, H. C. Crawford, Y. M. Shah and C. A. Lyssiotis, *eLife*, 2022, **11**, e73245.
29 S. E. Day, M. I. Kettunen, F. A. Gallagher, D.-E. Hu, M. Lerche, J. Wolber, K. Golman, J. H. Ardenkjaer-Larsen and K. M. Brindle, *Nat. Med.*, 2007, **13**, 1382–1387.
30 C. E. Christensen, M. Karlsson, J. R. Winther, P. R. Jensen and M. H. Lerche, *J. Biol. Chem.*, 2014, **289**, 2344–2352.
31 S. Meier, M. Karlsson, P. R. Jensen, M. H. Lerche and J. Ø. Duus, *Mol. Biosyst.*, 2011, **7**, 2834–2836.
32 P. R. Jensen, M. R. A. Matos, N. Sonnenschein and S. Meier, *Anal. Chem.*, 2019, **91**, 5395–5402.
33 D. P. Cistola, D. M. Small and J. A. Hamilton, *J. Lipid Res.*, 1982, **23**, 795–799.
34 P. R. Jensen and S. Meier, *The Analyst*, 2016, **141**, 823–826.
35 P. R. Jensen and S. Meier, *Chem. Commun.*, 2016, **52**, 2288–2291.
36 W. Lu, X. Su, M. S. Klein, I. A. Lewis, O. Fiehn and J. D. Rabinowitz, *Annu. Rev. Biochem.*, 2017, **86**, 277–304.
37 J. K. Nicholson, P. J. D. Foxall, Manfred. Spraul, R. Duncan. Farrant and J. C. Lindon, *Anal. Chem.*, 1995, **67**, 793–811.
38 K. N. Timm, J. Hartl, M. A. Keller, D.-E. Hu, M. I. Kettunen, T. B. Rodrigues, M. Ralser and K. M. Brindle, *Magn. Reson. Med.*, 2015, **74**, 1543–1547.
39 J. O. Park, S. A. Rubin, Y.-F. Xu, D. Amador-Noguez, J. Fan, T. Shlomi and J. D. Rabinowitz, *Nat. Chem. Biol.*, 2016, **12**, 482–489.
40 M. Otsuka, T. Mine, E. Ohuchi and S. Ohmori, *J. Biochem. (Tokyo)*, 1996, **119**, 246–251.
41 B. O. Petersen, O. Hindsgaul and S. Meier, *Analyst*, 2013, **139**, 401–406.
42 M. Bøjstrup, B. O. Petersen, S. R. Beeren, O. Hindsgaul and S. Meier, *Anal. Chem.*, 2013, **85**, 8802–8808.
43 C. S. Clendinen, B. Lee-McMullen, C. M. Williams, G. S. Stupp, K. Vandenborne, D. A. Hahn, G. A. Walter and A. S. Edison, *Anal. Chem.*, 2014, **86**, 9242–9250.
44 G. H. J. Park, S.-H. Yang and H.-M. Baek, *PLOS ONE*, 2018, **13**, e0203379.
45 R. J. Gillies, K. Ugurbil, J. A. den Hollander and R. G. Shulman, *Proc. Natl. Acad. Sci.*, 1981, **78**, 2125–2129.
46 H. Pelicano, D. S. Martin, R.-H. Xu and P. Huang, *Oncogene*, 2006, **25**, 4633–4646.
47 A. F. Abdel-Wahab, W. Mahmoud and R. M. Al-Harizy, *Pharmacol. Res.*, 2019, **150**, 104511.
48 P. R. Jensen, F. Sannelli, L. T. Stauning and S. Meier, *Chem. Commun.*, 2021, **57**, 10572–10575.
49 M. H. Lerche, P. R. Jensen, M. Karlsson and S. Meier, *Anal. Chem.*, 2015, **87**, 119–132.
50 H. Allouche-Arnon, T. Wade, L. F. Waldner, V. N. Miller, J. M. Gomori, R. Katz-Brull and C. A. McKenzie, *Contrast Media Mol. Imaging*, 2013, **8**, 72–82.
51 M. Mishkovsky, B. Anderson, M. Karlsson, M. H. Lerche, A. D. Sherry, R. Gruetter, Z. Kovacs and A. Comment, *Sci. Rep.*, 2017, **7**, 11719.
52 E. Can, M. Mishkovsky, H. A. I. Yoshihara, N. Kunz, D.-L. Couturier, U. Petrausch, M.-A. Doucey and A. Comment, *Sci. Rep.*, 2020, **10**, 200.
53 M. Liu and C. Hilty, *Anal. Chem.*, 2018, **90**, 1217–1222.
54 E. Miclet, D. Abergel, A. Bornet, J. Milani, S. Jannin and G. Bodenhausen, *J. Phys. Chem. Lett.*, 2014, **5**, 3290–3295.
55 T. B. Rodrigues, E. M. Serrao, B. W. C. Kennedy, D.-E. Hu, M. I. Kettunen and K. M. Brindle, *Nat. Med.*, 2014, **20**, 93–97.
56 S. Meier, P. R. Jensen and J. Ø. Duus, *FEBS Lett.*, 2011, **585**, 3133–3138.
57 T. W.-M. Fan and A. N. Lane, *Prog. Nucl. Magn. Reson. Spectrosc.*, 2016, **92–93**, 18–53.
58 J. L. Slonczewski, B. P. Rosen, J. R. Alger and R. M. Macnab, *Proc. Natl. Acad. Sci.*, 1981, **78**, 6271–6275.
59 T. Harris, H. Degani and L. Frydman, *NMR Biomed.*, 2013, **26**, 1831–1843.
60 F. A. Gallagher, M. I. Kettunen, S. E. Day, D.-E. Hu, J. H. Ardenkjær-Larsen, R. in 't Zandt, P. R. Jensen, M. Karlsson, K. Golman, M. H. Lerche and K. M. Brindle, *Nature*, 2008, **453**, 940–943.
61 K. O. Alfarouk, S. B. M. Ahmed, R. L. Elliott, A. Benoit, S. S. Alqahtani, M. E. Ibrahim, A. H. H. Bashir, S. T. S. Alhoufie, G. O. Elhassan, C. C. Wales, L. H. Schwartz, H. S. Ali, A. Ahmed, P. F. Forde, J. Devesa, R. A. Cardone, S. Fais, S. Harguindey and S. J. Reshkin, *Metabolites*, 2020, **10**, 285.
62 V. Cossu, M. Bonanomi, M. Bauckneht, S. Ravera, N. Righi, A. Miceli, S. Morbelli, A. M. Orengo, P. Piccioli, S. Bruno, D. Gaglio, G. Sambuceti and C. Marini, *Sci. Rep.*, 2020, **10**, 22111.
63 J. Whitburn, S. R. Rao, E. V. Morris, S. Tabata, A. Hirayama, T. Soga, J. R. Edwards, Z. Kaya, C. Palmer, F. C. Hamdy and C. M. Edwards, *Sci. Adv.*, 2022, **8**, eabf9096.
64 R. E. Hurd, Y.-F. Yen, D. Mayer, A. Chen, D. Wilson, S. Kohler, R. Bok, D. Vigneron, J. Kurhanewicz, J. Tropp, D. Spielman and A. Pfefferbaum, *Magn. Reson. Med.*, 2010, **63**, 1137–1143.
65 N. M. Zacharias, H. R. Chan, N. Sailasuta, B. D. Ross and P. Bhattacharya, *J. Am. Chem. Soc.*, 2012, **134**, 934–943.
66 P. R. Jensen, S. C. Serra, L. Miragoli, M. Karlsson, C. Cabella, L. Poggi, L. Venturi, F. Tedoldi and M. H. Lerche, *Int. J. Cancer*, 2015, **136**, E117–E126.
67 C. Harrison, C. Yang, A. Jindal, R. J. DeBerardinis, M. A. Hooshyar, M. Merritt, A. Dean Sherry and C. R. Malloy, *NMR Biomed.*, 2012, **25**, 1286–1294.

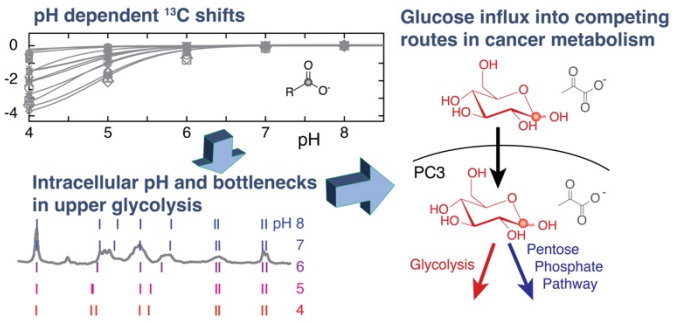

TOC Figure